Responses of atmospheric circulation to sea surface temperature anomalies in the South China Sea

M. Zhou and G. Wang

State Key Laboratory of Satellite Ocean Environment Dynamics, Second Institute of Oceanography, State Oceanic Administration, Hangzhou 310012, China

Correspondence to: Guihua Wang (gwang@sio.org.cn)

Abstract

The sea surface temperature (SST) anomalies in the South China Sea (SCS) and their influences on global atmospheric circulation were studied. The results of a simple atmospheric model suggested that the SCS SST anomalies can induce several barotropic wave trains from the SCS to other regions such as North America, high latitudes of the Southern Hemisphere and the Mediterranean. The baroclinic stream function anomalies from the simple model showed an anticyclonic vortex pair in East Asia and the southern tropical Indian Ocean and a cyclonic vortex in the North Pacific and the Southwest Pacific. It is suggested that the spatial pattern of SST anomalies in the SCS can affect the magnitude of stream function anomalies, although it cannot affect the spatial pattern of atmospheric circulation.

1. Introduction

The South China Sea (SCS, 0-25°N, 100-125°E) is the largest marginal sea in the Northwest Pacific. The sea surface temperature (SST) in the SCS shows a significant seasonal cycle. The climatological SSTs in summer (June to August) and winter (December to February) over the SCS are shown in Fig. 1. The SST in summer is mostly above 28°C, with a pronounced cold tongue veering off central Vietnam (Fig. 1a). During winter, the SST is cold in the northwest and warm in the southeast of the SCS (Fig. 1b).

The SST in the SCS had a robust warming trend during past several decades (Luo et al., 1986; Fang et al., 2006; Xie et al., 2010; Zhang et al., 2010; Liu and Zhang, 2013). Based on the Optimum Interpolation Sea Surface Temperature (OISST) dataset, Fang et al. (2006) founded that the SST in the SCS had a positive linear trend of 5°C $(100yr)^{-1}$ during 1993-2003. The summer and winter SST trends in the SCS from 1982 to 2011 are also shown in Fig. 1. Whether in summer or in winter, the SCS warming trend is significant, with1.64°C $(100yr)^{-1}$ in summer and 2.04°C $(100yr)^{-1}$ in winter. The maximum SST trend can exceed 9.50°C $(100yr)^{-1}$. During summer, the larger warming is in the western SCS and the smaller warming in the eastern SCS. During winter, the pattern changes to the larger warming in the eastern SCS and the smaller warming in the western SCS. It should be noted that the SCS warming was faster than the global average, and that the warming was the largest between 0-20°N globally.

Many studies focused on the effects of positive SST anomalies in the SCS on precipitation and climate in China (Zhang et al., 2003; Fong et al., 2004; Roxy and Tanimoto, 2012). According to Zhang et al. (2003), the positive SST anomaly in summer with respect to the seasonal climatology in the SCS was followed by anomalous southward wind, and then more moisture was transported to South China, which resulted in floods in the Yangtze River Valley. Fong et al. (2004) suggested that the SCS surface warming can enhance latent and sensible heat fluxes from the sea surface and result in a cyclonic circulation anomaly in the lower troposphere and an anti-cyclonic circulation anomaly in the upper troposphere, which can then affect the climate of South China. Roxy and Tanimoto (2012) pointed out that the positive SST anomalies over the SCS tended to form a favorable condition for convective activity and enhanced the northward propagating precipitation anomalies during the SCS summer monsoon. Other studies showed that

the SST anomalies in the SCS can influence SCS monsoon onset (Johnson and Ciesielski, 2002; Ding et al., 2004; Lestari and Iwasaki, 2006) and its variability (Liu and Xie, 1999; Lestari et al., 2011; Roxy and Tanimoto, 2012).

Teleconnections are well-known and well-studied (Wallace and Gutzler 1981; Huang, 1984; Nitta, 1986; Nitta, 1987). A local change in the surface boundary condition can have far reaching influences in a remote area. For example, the diabatic heating anomaly over the central equatorial Pacific during ENSO (El Niño-Southern Oscillation) can excite a stationary barotropic Rossby wave train propagating into extratropical regions. This teleconnection is known as the Pacific-North American (PNA) pattern (Wallace and Gutzler, 1981) in the Northern Hemisphere. Nitta (1987) found another teleconnection between abnormal convective activity over the tropical western North Pacific and atmospheric circulation anomalies over the mid-latitude of East Asia in summer, which was named the Pacific-Japan (PJ) pattern.

These studies mostly discussed how the SST in the SCS affected the local climate. The teleconnection between the SCS and global atmosphere circulation is not clear. In this paper, we use a simple atmospheric model to discuss this teleconnection. The rest of this paper is organized as follows. Section 2 describes the data and model used in this study. The results obtained from the simple atmospheric model are presented in Sect. 3. Summary and discussion are provided in Sect. 4.

2. Data and model

2.1 Data and method

Two datasets are used in this study. The climatological stream functions are from the National Centers for Environmental Prediction/National Center for Atmospheric Research (NECP/NCAR) reanalysis, which is available on a 2.5° by 2.5° grid (Kalnay et al., 1996). The OISST analysis product is from the National Oceanic and Atmospheric Administration (NOAA), which has the spatial resolution of 0.25° by 0.25° (Reynolds et al., 2002). The period of the two datasets used is from 1982 to 2011.

The basic mean flows are represented by the stream functions at 250 and 750 hPa from the monthly NCEP/NCAR reanalysis. The stream functions at 750 hPa are constructed by linear interpolation from standard pressure levels, as 750 hPa is not a standard pressure level. Since the

model atmosphere is simplified to two levels (centered at 250 and 750 hPa), the stream functions can be separated into barotropic and baroclinic components as follows:

$$\psi_{barotropic} = 0.5 \cdot (\psi_{250hPa} + \psi_{750hPa}), \quad (1)$$

$$\psi_{baroclinic} = 0.5 \cdot (\psi_{250hPa} - \psi_{750hPa}), \quad (2)$$

where ψ stands for stream function.

Figure 2 shows the spatial pattern of mean barotropic stream function (Fig. 2a) and baroclinic stream function (Fig. 2b) from 1982 to 2011. Whether barotropic or baroclinic stream function, it was the westerly in high latitudes. In the tropical regions, the flows fluctuated due to strong convections.

2.2 Atmospheric model

We use a simple atmospheric model developed by Lee et al. (2009) to simulate global atmospheric circulation. This is a steady-state, two-level (centered at 250 and 750 hPa) spherical-coordinate primitive equation model, linearized about prescribed background mean flows. The model uses triangular 18 truncations for its horizontal grids. The formulation is similar to that of the multi-level linear baroclinic model used by Hoskins and Simmons (1975) and others, but its governing equations are greatly simplified by employing Gill's (1980) simple thermodynamic equation. Detailed description of the simple model can be found in Lee et al. (2009). This model successfully simulated local and remote responses of the atmosphere to tropical heating anomalies (Lee et al., 2009; Wang et al., 2010; Zheng et al., 2013). In this study, we use the basic mean flows as the initial conditions and heating in the SCS as the forcing condition to drive this model.

2.3 Experiments setup

To see how basin-scale SST anomalies affect the atmospheric circulation, we set six experiments:

Case 1: uniform heating in the SCS,

Case 2: heating decreased northward in the SCS to consider the differences of meridional solar radiation,

Case 3: heating pattern similar to the SST winter pattern,

Case 4: heating pattern similar to the SST summer pattern,

Case 5: summer SST warming trend heating pattern,

Case 6: winter SST warming trend heating pattern,

Case 1 and Case 2 are for testing the effects of the difference of meridional solar radiation. Case 3 and case 4 are for testing the effects of seasonal SST anomalies in the SCS. As shown in Fig. 1, the SST in winter is cooler in the northwest and warmer in the southeast SCS, which is used in Case 3, while the pronounced cold tongue veering off central Vietnam in summer is included in Case 4. Heating patterns derived from SST anomalies for these four experiments are summarized in Fig. 3. Case 5 and Case 6 are for testing the effects of the SST warming differences in the zonal direction on atmospheric circulation. All the calculations are listed in Table 1. Note the total heat input is same for the six experiments to ensure comparability.

3. Results

3.1 Influence of SST anomalies in the meridional direction

Figure 4a shows the barotropic stream function anomalies from Case 1. There are three robust waves. The first one is from the SCS to North America through the northwestern Pacific, which is somewhat similar to the classical PNA pattern (Wallace and Gutzler, 1981; Nitta, 1986; Huang, 1984). The second one is from the SCS to high latitudes of the Southern Hemisphere across the equator. As shown by Wang et al. (2010), the background vertical wind shear is important in converting energy from the heating-induced baroclinic flow anomalies into barotropic motions near the heating source. The barotropic anomalies in turn interact with the mean westerly wind to transmit the barotropic signals to the high latitudes of the Southern Hemisphere. Note another small wave train is from the SCS to the Mediterranean. According to the classical theory of energy dispersion (Yeh, 1949) and the great circle theory (Hoskins and Karoly, 1981), disturbances produced by local heating can spread westward.

The baroclinic stream function anomalies from the simple model show an anticyclonic vortex pair in East Asia and southern tropic Indian Ocean (Fig. 4b). Accordingly, a cyclonic vortex pair appears in the north and southwest Pacific, quite similar to the Matsuno–Gill model (Gill, 1980)

and is consistent with the results of Smagorinsky (1953) and Heckley and Gill (1984). The response of atmospheric circulation to the heating anomaly in the SCS suggests that the Gill dynamics is at work.

We calculate the seasonal cycle of the air-sea temperature difference (figures not shown here). It suggests that atmosphere reduces heat loss to the ocean during the boreal winter in the northern SCS and increases heat flux from the ocean during the summer in the northern SCS. This is supported by He and Wu (2013) that the boreal winter SST in the northern SCS is independent from the atmospheric condition; it gives an opportunity to look at the observational data sets and find support for the described teleconnections. The correlations between the winter SST anomalies in the northern SCS and the barotropic/baroclinic stream functions are calculated. The correlation in Fig. 5a shows two waves: one from the SCS to North America and the other from the SCS to the Southern Hemisphere. The correlation in Fig. 5b shows positive anomalies in East Asia and the Southwest Pacific and negative anomalies in the North Pacific and southern tropical Indian Ocean. These support the described teleconnections between SCS SST and the global atmospheric circulation.

The barotropic and baroclinic stream function anomalies for Cases 2-4 are basically the same as those for Case 1, which indicates that the positive heating anomalies in the SCS can all induce three waves in the barotropic stream function and two vortex pairs in the baroclinic stream function regardless of the spatial pattern of the heating. The amplitudes are slightly different in the four experiments. For the PNA-like-pattern wave train and the Southern-Hemisphere wave train, the barotropic stream functions in Cases 1 and 4 are weaker than those in Cases 2 and 3 in terms of anticyclonic anomalies, but they are stronger than those in Cases 2 and 3 in terms of cyclonic anomalies (Fig. 6a). Conversely, the baroclinic stream functions of Cases 1 and 4 are weaker than those in Cases 2 and 3 in terms of cyclonic anomalies, but are stronger than those in Cases 2 and 3 in terms of anticyclonic anomalies (Fig. 6b). The differences among the four cases suggest that the spatial pattern of SST anomalies can affect the magnitudes of both stream functions, although it cannot affect the spatial pattern of the atmospheric circulation. The role of asymmetric heating in influencing atmosphere circulation can also be seen in many studies such as Fu et al. (1980) and Dunkerton (1989).

3.2 Influence of SST anomalies in the zonal direction

The spatial patterns of the stream function anomalies for Cases 5 and 6 are also quite similar to those in Case 1 for both barotropic and baroclinic components. For the PNA-like-pattern wave train or the Southern-Hemisphere wave train, the barotropic stream function in Case 5 is weaker than that in Case 6 in terms of cyclonic anomalies, but is stronger than that in Case 6 in terms of anticyclonic anomalies (Fig. 7a). Conversely, the baroclinic stream function in Case 5 is weaker than that in Case 6 in terms of anticyclonic anomalies, but is stronger than that in Case 6 in terms of cyclonic anomalies (Fig. 7b). As shown in Fig. 1, the larger warming trend is in the western SCS in summer but in the eastern SCS in winter. The difference between Cases 5 and 6 suggests that the larger warming trend in the western (eastern) SCS heating pattern can weaken (strengthen) the cyclonic anomalies and strengthen (weaken) the anticyclonic anomalies in the barotropic component. On the contrary, the larger warming trend in the western (eastern) SCS heating pattern can strengthen (weaken) cyclonic anomalies and weaken (strengthen) the anticyclonic anomalies in the baroclinic component. It also suggests that the spatial pattern of SST trend can affect the magnitude of stream functions, although it cannot affect the spatial pattern of atmospheric circulation.

4. Summary and discussion

In this study, the influences of SST anomalies in the SCS on global atmospheric circulation were studied. The results of the simple atmospheric model suggested that the SCS heating can induce a barotropic wave train from the SCS to the Northwest Pacific Ocean and North America, which is somewhat similar to the classical PNA pattern. Simultaneously, the SCS heating can induce a barotropic wave train from the SCS to high latitudes of the Southern Hemisphere. In particular, we noticed a weak barotropic wave train from the western SCS to the Mediterranean. The baroclinic stream function anomalies from the simple model showed an anticyclonic vortex pair in East Asia and the southern tropic Indian Ocean and a cyclonic vortex in the North Pacific and the Southwest Pacific. The stream function anomalies of the barotropic and baroclinic components for all six cases are basically the same, with slight differences in amplitude. It suggests that the spatial pattern of heating can cause some differences in magnitude, but not in circulation patterns.

Our findings in this study may be important for both regional and global climate research. For example, we calculated the correlation between the northern SCS SST anomalies and the rainfall. The correlation pattern is quiet similar to Fig. 4a, showing two waves: one from the SCS to North America and the other from the SCS to the Southern Hemisphere (figures not shown here); thus, this study may help to forecast climate-related events like rainfall in North America based on the SCS SST anomalies.

Because the two level model only considering Gill's (1980) simple thermodynamics equation is applied here, many dynamic/thermodynamic are ignored completely. Thus, a more complex atmospheric general circulation model is needed for further study.

Acknowledgments

The authors thank Dr. Sang-Ki Lee and Dr. Chunzai Wang for sharing the model code and helping to run the model. The authors are grateful to the two anonymous reviewers who have helped in improving the manuscript considerably. This study was supported by the National Basic Research Program of China and the National Natural Science Foundation of China.

References

Ding, Y. H., Li, C. Y., and Liu, Y. J.: Overview of the South China Sea monsoon experiment. Adv. Atmos. Sci., 21:3, 343-360, doi: 10.1007/BF02915563, 2004.

Dunkerton, T. J.: Nonlinear Hadley circulation driven by asymmetric differential heating [J]. J. Atmos. Sci., 46(7): 956-974, 1989.

Fang, G., H. Wei, Chen, Z., Wang, Y., Wang, X., and Li, C.: Trends and interannual variability of the South China Sea surface winds, surface height, and surface temperature in the recent decade. J. Geophys. Res., 111, C11S16, doi: 10.1029/2005JC003276, 2006.

Fong, S. K., Wu, C. S., Wang, A. Y., Ku, C. M., Hao, I. P., and Tong, T. N.: A numerical study of the effects of South China Sea SST anomalies on the climate in South China. Journal of Tropical Meteorology, 20:1, 32-38 (in Chinese), 2004.

Fu, K. Z., Wu, H. D., Fang, X. F., Wang, Y. K.: Asymmetric heating effects on the general circulation of atmosphere. Acta Meteorologica Sinica, 38:3, 205-218(in Chinese), 1980.

Gill, A. E.: Some simple solutions for heat-induced tropical circulation. Quart. J. Roy. Meteor. Soc., 106, 447–462, doi: 10.1002/qj.49710644905, 1980.

He, Z. Q., and Wu, R. G.: Seasonality of interannual atmosphere–ocean interaction in the South China Sea. J. Oceanogr, 69(6), 699-712. doi: 10.1007/s10872-013-0201-9, 2013.

Heckley, W. A., and Gill, A. E.: Some simple analytical solutions to the problem of forced equatorial long waves. Quart. J. Roy. Meteor. Soc., 110(463), 203-217. DOI: 10.1002/qj.49711046314, 1984

Hoskins, B. J., and Simmons, A. J.: A multi-layer spectral model and the semi-implicit method. Quart. J. Roy. Meteor. Soc., 101, 637–655, doi: 10.1002/qj.49710142918, 1975.

Hoskins, J. Brian, and Karoly, D. J.: The Steady Linear Response of a Spherical Atmosphere to Thermal and Orographic Forcing. J. Atmos. Sci., 38, 1179–1196, doi: http://dx.doi.org/10.1175/ 1520-0469(1981)038<1179:TSLROA>2.0.CO;2, 1981.

Huang, R. H.: The characteristics of the forced stationary planetary wave propagations in summer Northern Hemisphere. *Adv. Atmos. Sci.*, **1:1**, 84-94, doi: 10.1007/BF03187619, 1984.

Johnson, R. H. and Ciesielski, P. E.: Characteristics of the 1998 summer monsoon onset over the

northern South China Sea, J. Meteorol. Soc. Jpn. Ser. II, 80:4, 561-578, doi: http://dx.doi.org/10.2151/jmsj.80.561, 2002.

Kalnay, E., Kanamitsu, M., Kistler, R., Collins, W., Deaven, D., Gandin, L., Iredell, M., Saha, S., White, G., Woollen, J., Zhu, Y., Leetmaa, A., Reynolds, B., Chelliah, M., Ebisuzaki, W., Higgins, W., Janowiak, J., Mo, K. C., Ropelewski, C., Wang, J., Jenne, R., and Joseph, D.: The NCEP/NCAR 40-Year Reanalysis Project. Bull. Amer. Meteor. Soc., 77, 437–471,doi: http://dx.doi.org/ 10.1175/1520-0477(1996)077<0437:TNYRP>2.0.CO;2, 1996.

Lee, S. K., Wang, C. Z., and Mapes, B. E.: A Simple Atmospheric Model of the Local and Teleconnection Responses to Tropical Heating Anomalies. J. Climate, 22, 272–284, doi: http://dx.doi.org/10.1175 /2008JCLI2303.1, 2009.

Lestari, R. K., Watanabe, M., and Kimoto, M.: Role of air-sea coupling in the interannual variability of the South China Sea summer monsoon. J. Meteorol. Soc. Jpn. Ser. II, 89, 283-290, doi: http://dx.doi.org/10.2151/jmsj.2011-A18, 2011.

Lestari, R. K., and Iwasaki, T.: A GCM study on the roles of the seasonal marches of the SST and land-sea thermal contrast in the onset of the Asian summer monsoon. J. Meteorol. Soc. Jpn. Ser. II, 84(1), 69-83, 2006.

Liu, W. T., and Xie, X.: Space-based observations of the seasonal changes of South Asian monsoons and oceanic response, Geophys. Res. Lett., 26, 1473–1476, doi: 10.1029/2003JC001867, 1999.

Liu, Q., and Zhang, Q.: Analysis on long-term change of sea surface temperature in the China Seas. J. Ocean Univ. China, 12:2, 295-300.doi: 10.1007/s11802-013-2172-2, 2013.

Luo, S. H., and Jin, Z. H.: Statistical analyses for sea surface temperature over the South China Sea, behavior of subtropical high over the west pacific and monthly mean rainfall over the Chang Jiang middle and lower reaches. Journal of Atmospheric Sciences. 10.4, 409-418 (in Chinese), 2006.

Nitta, T.: Long-term variations of cloud amount in the western Pacific region. J. Meteorol. Soc. Jpn., 64:3, 373-390, 1986.

Nitta, T.: Convective activities in the tropical western pacific and their impact on the northern hemisphere circulation. J. Meteorol. Soc. Jpn., 65, 373-390,1987.

Reynolds, R. W., Rayner, N. A., Smith, T. M., Stokes, D. C., and Wang, W. Q.: An improved in

situ and satellite SST analysis for climate, J. Clim., 15:13, 1609–1625, doi: http://dx.doi.org/10.1175/1520-0442(2002)015 <1609:AIISAS>2.0.CO;2, 2002.

Roxy, M., and Tanimoto, Y.: Influence of sea surface temperature on the intraseasonal variability of the South China Sea summer monsoon. Clim. Dyn., 39:5, 1209-1218, doi: 10.1007/s00382-011-1118-x, 2012.

Smagorinsky, J.: The dynamical influence of large-scale heat sources and sinks on the quasi-stationary mean motions of the atmosphere. Q. J. R. Meteorol. Soc., 79, 342–366. doi: 10.1002/qj.49707934103, 1953.

Wallace, J. M., and Gutzler, D. S.: Teleconnections in the geopotential height field during the Northern Hemisphere winter. Mon. Wea. Rev., 109, 784–812, doi: http://dx.doi.org/10.1175/1520-0493(1981)109<0784: TITGHF>2.0.CO;2, 1981.

Wang, C. Z., Lee, S. K., Mechoso, C. R.: Interhemispheric Influence of the Atlantic Warm Pool on the Southeastern Pacific. J. Climate, 23:2, 404-418, doi: http://dx.doi.org/10.1175/2009JCLI3127.1, 2010.

Xie, S. P., Deser, C., Vecchi, A. G., Ma, J., Tend, H., and Wittenberg, A. T.: Global warming pattern formation: sea surface temperature and rainfall. J. Climate, 23: 966-986, doi: http://dx.doi.org/10.1175/2009JCLI3329.1, 2010.

Yeh, T.: ON ENERGY DISPERSION IN THE ATMOSPHERE. J. Meteor., 6, 1–16, doi: http://dx.doi.org/10.1175/1520-0469(1949)006<0001:OEDITA>2.0.CO;2, 1949.

Zhang Q., Liu, P., and Wu, G. X.: The relationship between the flood and drought over the lower reach of the Yangtze River Valley and the SST over the Indian Ocean and the South China Sea. Journal of Atmospheric Sciences, 27 (6), 992-1006 (in Chinese) , 2003.

Zhang, L. P., Wu, L. X., Lin, X. P., and Wu, D. X.: Modes and mechanisms of sea surface temperature low-frequency variations over the coastal China seas. J. Geophys. Res., 115, C08031, doi: 10.1029/2009JC006025, 2010.

Zheng, J., Liu, Q. Y., Wang, C. Z., and Zheng, X. T.: Impact of heating anomalies associated with rainfall variations over the indo-western Pacific on Asian atmospheric circulation in winter. Clim. Dyn., 40, 2023-2033, doi: 10.1007/s00382-012-1478-x, 2013.

Table 1. The heat forcing Q at each grid for Cases 1-6.

Exp.	Heat forcing in the SCS	Description
Case 1	$Q(i, j)=Q_0^*$	Uniform heating
Case 2	$Q(i, j)=Q_0 \cdot (25-lat(i, j))/12.5$	Heating less in the north
Case 3	$Q(i, j)=Q_0 \cdot ((25-lat(i, j))+(125-lon(i, j)))/25$	Similar to SST winter pattern
Case 4	$Q(i, j)=Q_0 \cdot ((12.5-lat(i, j))^2/10+lon(i, j)-100)/18.125$	Similar to SST summer pattern
Case 5	$Q(i, j)=Q_0 \cdot$ summer SST trends pattern/1.64	summer SST trends pattern
Case 6	$Q(i, j)=Q_0 \cdot$ winter SST trends pattern/2.04	winter SST trends pattern
		$^*Q_0=1.16\times10^{-2}$ W kg^{-1} (1 °C day^{-1})

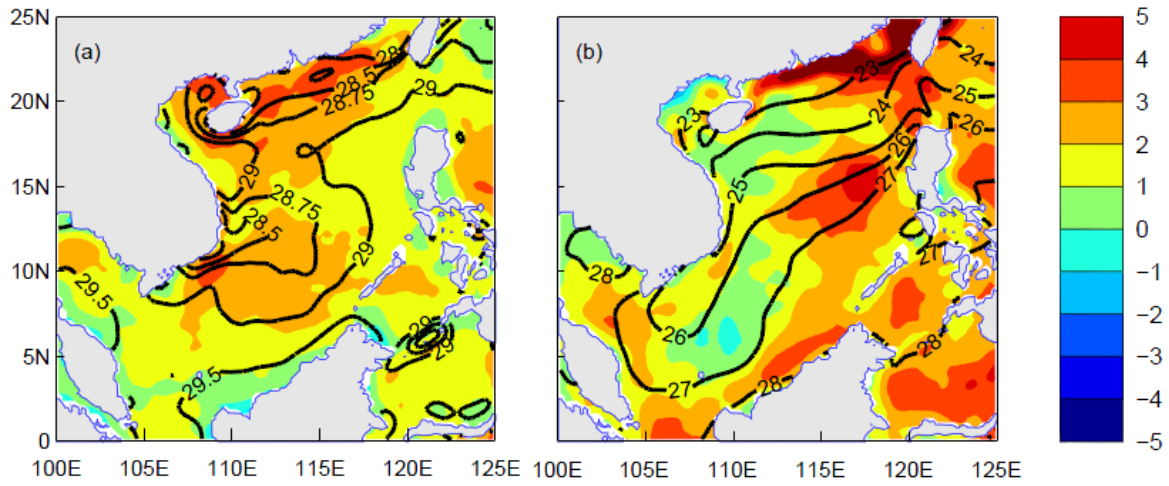

Figure 1. (a) Summer- and (b) winter-mean SST (contours; units: $^{\circ}$C) and SST trends (color shading; units: $^{\circ}$C (100yr)$^{-1}$) in the SCS from 1982 to 2011.

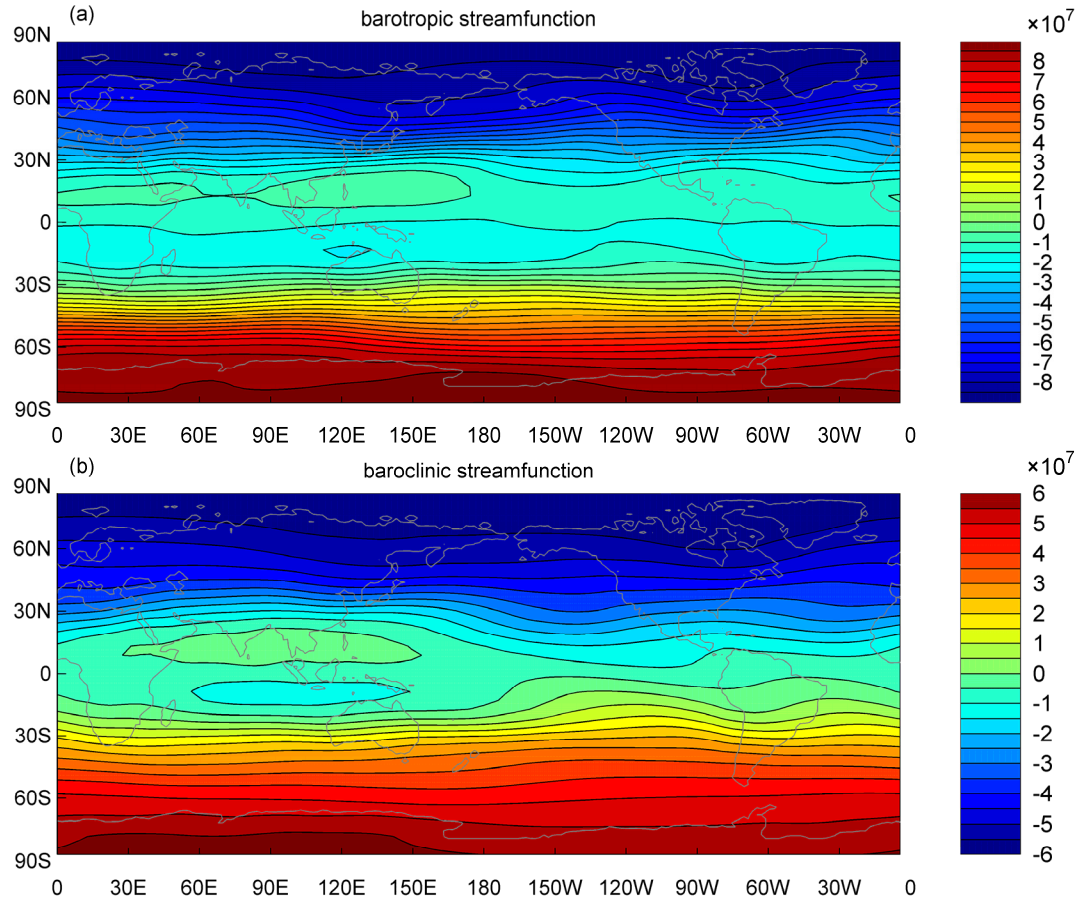

Figure 2. (**a**) Barotropic and (**b**) baroclinic stream functions of the climatology. The contour interval is 5.0×10^{6} m^{2} s^{-1}.

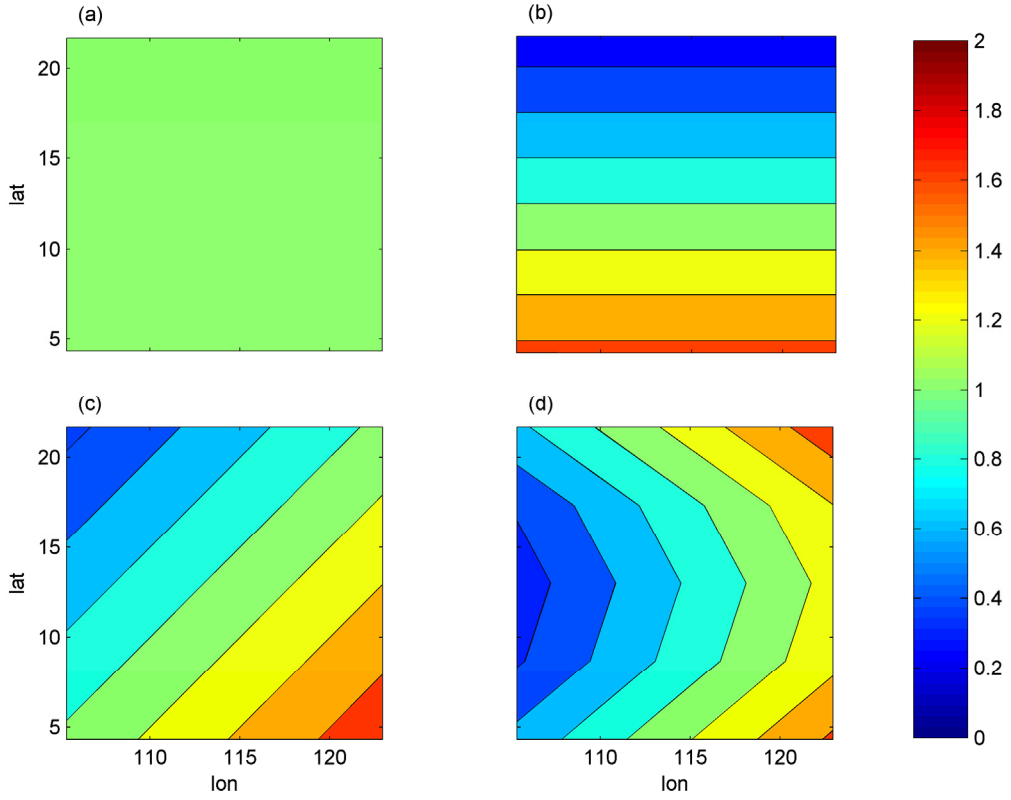

Figure 3. Spatial patterns of heat forcing Q for Cases 1-4 (**a-d**, units: Q_0).

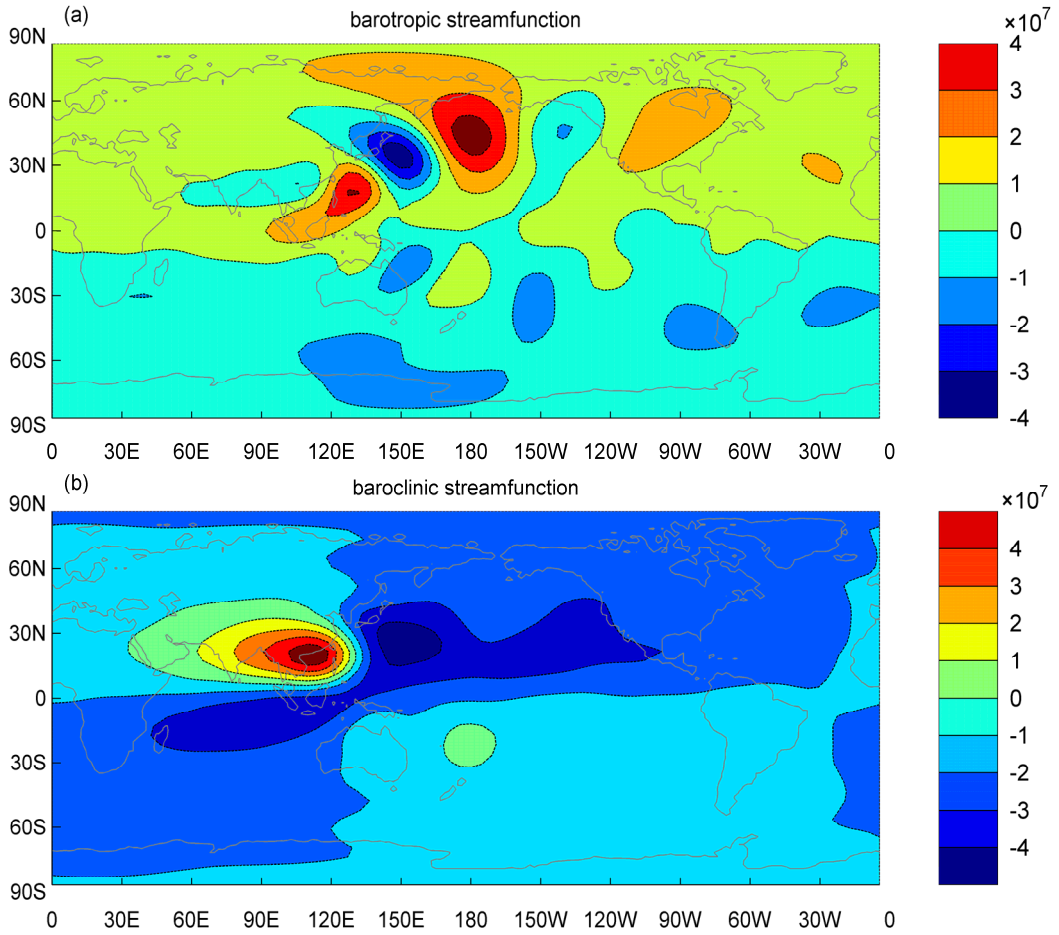

Figure 4. Barotropic (**a**) and baroclinic (**b**) stream function anomalies for Case 1. The contour interval is 1×10^6 m^2 s^{-1}.

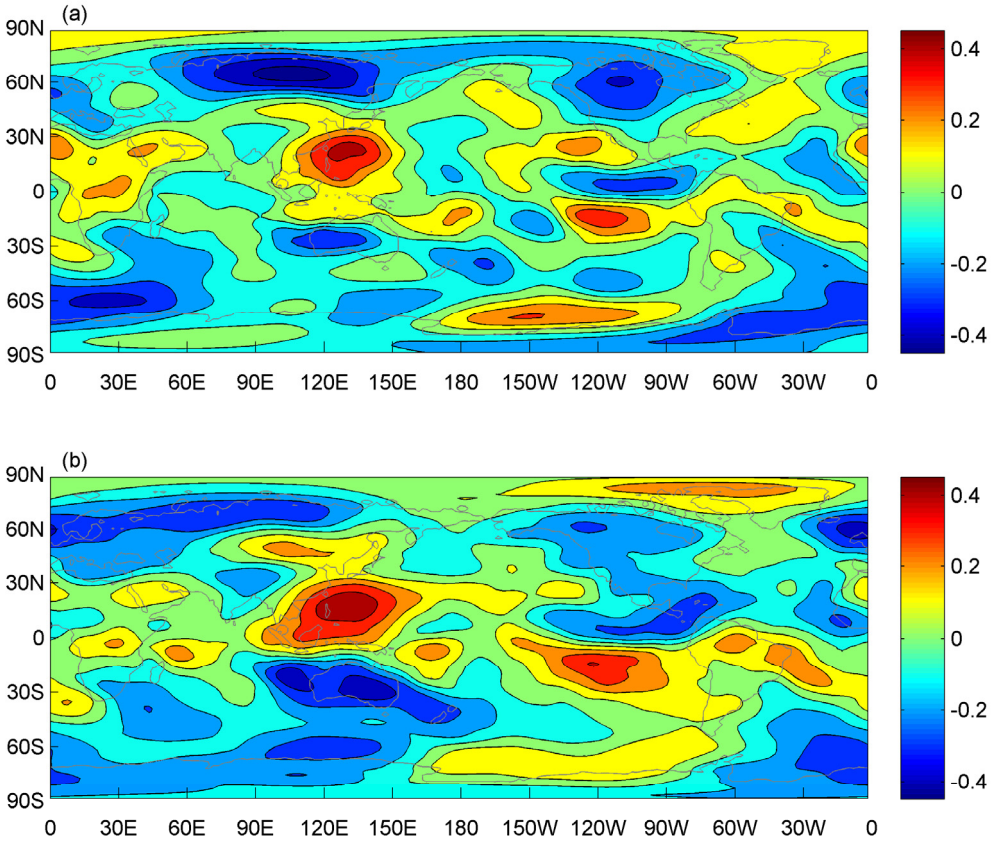

Figure 5. Lag correlation maps (lag day=15 days) of the northern SCS (110–121°E, 12–23°N) SST anomalies in winter (October 2003 to March 2004) with global barotropic stream function (**a**) and baroclinic stream function (**b**).

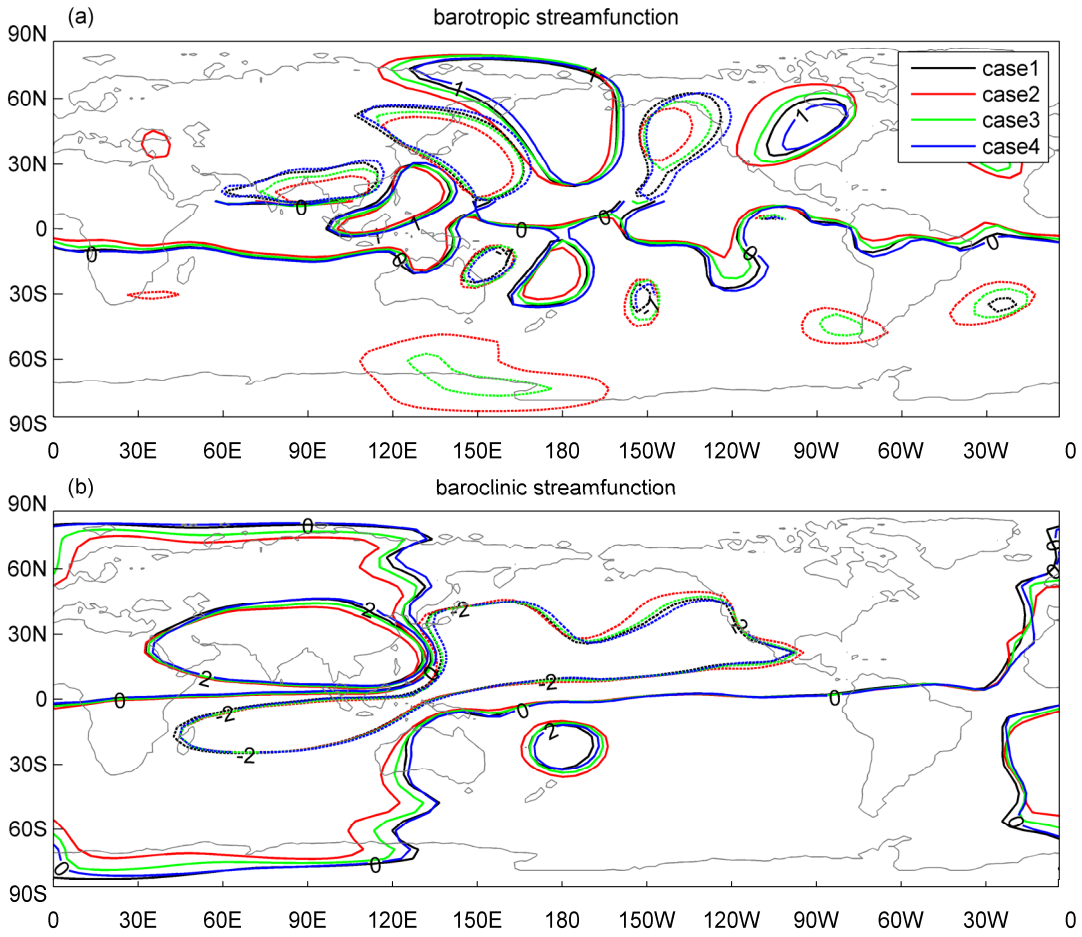

Figure 6. (**a**) Barotropic and (**b**) baroclinic stream function anomalies (units: $10^6 m^2 s^{-1}$) for Cases 1-4, with the black, red, green, and blue contours are stream function anomalies for Cases 1, 2, 3, and 4, respectively. The contour interval is 2×10^6 m^2 s^{-1}.

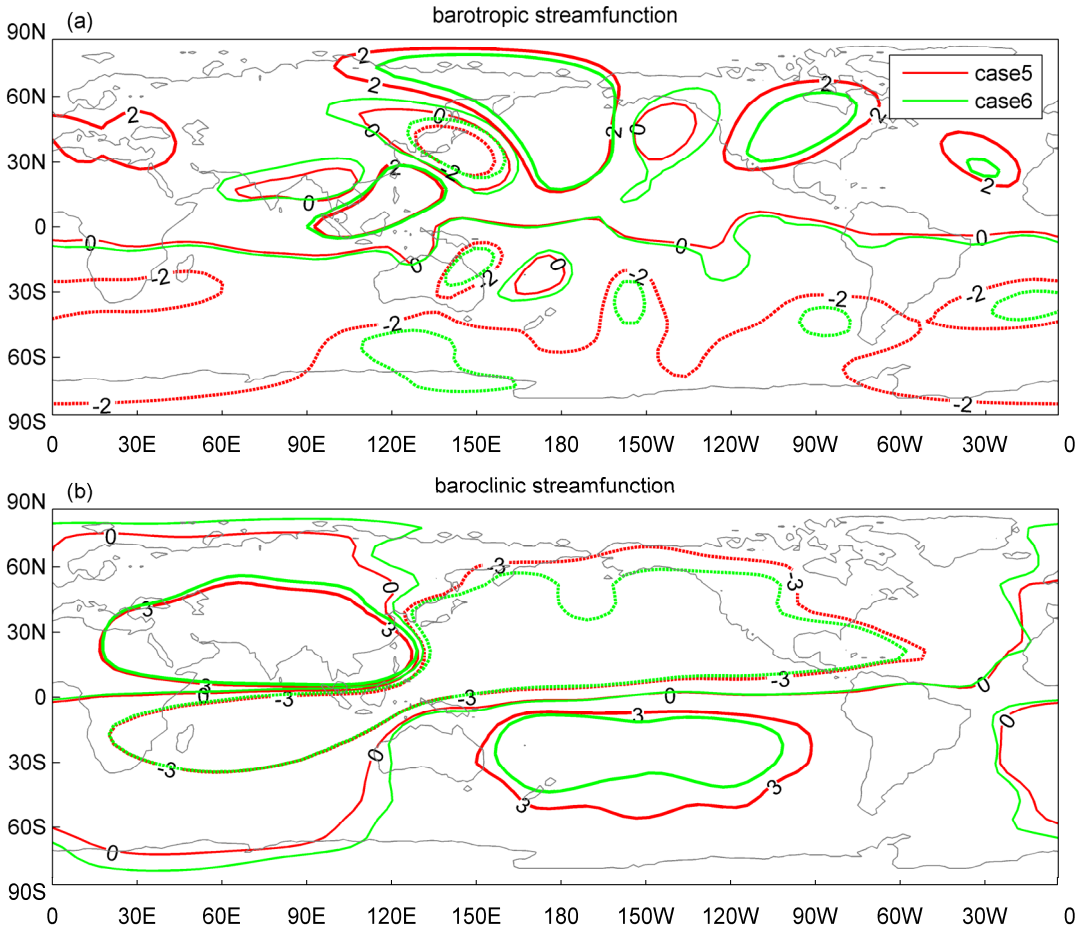

Figure 7. (**a**) Barotropic and (**b**) baroclinic stream function anomalies (10^6 m^2 s^{-1}) for Cases 5 (red) and 6 (green). The contour interval is 2×10^6 m^2 s^{-1} in the top panel and 3×10^6 m^2 s^{-1} in the bottom panel.